A Robust Dead-Reckoning Pedestrian Tracking System with Low Cost Sensors

Yunye Jin, Hong-Song Toh, Wee-Seng Soh, and Wai-Choong Wong
Department of Electrical and Computer Engineering
National University of Singapore
Email:{g0700214, u0705596, elesohws, elewwcl}@nus.edu.sg

***Abstract*—The emergence of personal mobile device with low cost sensors, such as accelerometer and digital compass, has made dead-reckoning (DR) an attractive choice for indoor pedestrian tracking. In this paper, we propose a robust DR pedestrian tracking system on top of such commercially accessible sensor sets capable of DR. The proposed method exploits the fact that, multiple DR systems, carried by the same pedestrian, have stable relative displacements with respect to the center of motion, and therefore to each other. We first formulate the robust tracking task as a generalized maximum a posteriori sensor fusion problem, and then we narrow it to a simple computation procedure with certain assumptions. A prototype is implemented and evaluated with a benchmark system that collects ground truth efficiently and accurately. In a practical indoor testbed, the proposed scheme has exhibited robust tracking performance, with reduction in average tracking error up to 73.7%, compared to traditional DR tracking methods.**

***Keywords*-Robust pedestrian tracking, dead-reckoning, location estimation, maximum a posteriori.**

I. Introduction

The ability to accurately track a user's location in urban and indoor areas has many applications in the healthcare, logistic, and entertainment industries. The Global Positioning System (GPS) service is either blocked or severely affected by multipath propagation in such environments. On the other hand, cellular-network-based localization schemes typically deliver an accuracy of hundreds of meters [1], which is unacceptable for many real-world applications.

In order to provide practical pedestrian tracking services with accuracy below room level, many approaches have been proposed, utilizing various technologies. Received signal strength (RSS)-based fingerprinting systems [2], [3] require an off-line training phase in order to build a "radio-map" of RSS. This approach is not only labor-intensive but also vulnerable to real-time environmental changes. On the other hand, practical range-based trilateration systems in the indoor environment estimate target location by distance measurements between the target device and each of the infrastructure nodes, through technologies such as ultrasound [4] and Wi-Fi [5], [6]. This approach requires dense deployment of infrastructure sensors in order to provide line-of-sight (LoS) coverage everywhere in the service area, which incurs high hardware cost. A similar problem is present in real-time adaptive systems such as [7], in which active "landmark" nodes are installed in the service area to provide real-time mappings from RSS to location.

In contrast to the afore-mentioned approaches, in which both the target device and the infrastructure deployment are indispensable, the dead-reckoning (DR) tracking scheme is almost self-contained in the target device alone (except for the initialization phase). A typical DR system consists of motion sensors, such as accelerometers, whose readings are used to estimate displacements by double integration. A major draw-back of such a system is that, the errors in the estimated displacement accumulate quickly over time because of the double integration of noisy sensor readings.

In order to reduce the cumulative tracking error in pedestrian DR systems, the "zero velocity update" (ZUPT) algorithm has been proposed [8]. This algorithm exploits an intrinsic property of pedestrian walking: the bottom of the sole has static contact with the floor which results in zero acceleration and velocity during a certain phase of each step taken. Therefore, any non-zero acceleration or velocity computed from the noisy sensor measurements during this particular phase should be eliminated because they must be the results of the accumulated error. This algorithm effectively reduces errors for pedestrian DR systems. However, the extra hardware cost of such a sensor module and the cumbersomeness of wearing such a module on the foot limits this algorithm only to special types of pedestrians, such as battle combatants and emergency responders.

Recent years have witnessed the emergence of personal mobile devices that come with DR-capable sensors, including both motion sensors, such as accelerometers, and orientation sensors, such as digital compass. Therefore, rather than purchasing and installing dedicated hardware modules, obtaining a personal DR tracking system can be made as simple as downloading a software application on such mobile devices for the end user. Although this approach is convenient and commercially accessible, it suffers from three disadvantages. First, these low cost sensors in mass-market devices are normally more noisy and the resulting DR estimation is subject to faster error accumulation. Second, such low cost sensors have lower rate in updating/refreshing their readings. Moreover, such mobile devices are usually placed in the user's pockets or mounted on belts, which usually do not experience any zero-velocity phase during a step. As a result of the arbitrary device placement, the ZUPT error reduction algorithm is rendered infeasible in this case.

Step-based DR tracking methods have been proposed for pedestrian tracking without ZUPT. Instead of performing

double integration, this approach exploits the patterns in variations of the accelerometer readings caused by steps. The heading orientation is obtained from the orientation sensor's reading if the sensor is properly aligned. Although excessive tracking error caused by double integration can be reduced, there can still be tracking errors caused by errors in step detection (mis-detection/false-detection), stride estimation, and orientation errors caused by distortion of magnetic fields by metal and magnetic objects.

In this paper, we propose a robust DR-based pedestrian tracking scheme implemented using low cost DR-capable sensors, embedded in commercially accessible mobile devices. The proposed scheme is based on the fact that, when two or more sets of such sensors are carried by the same walking pedestrian, they all have stable relative displacements with respect to the center of pedestrian motion, as well as small and limited local random motions. Therefore, relative displacements between these devices are also reasonably stable, which can be exploited to reduce the overall DR tracking error. We first formulate the robust tracking algorithm as a maximum a posteriori (MAP) sensor fusion problem in general. We then demonstrate that this algorithm can be specialized to a simple computation procedure by making certain assumptions. In order to verify the performance of this scheme, we implement a prototype of our proposed robust tracking system in commercially accessible devices, as well as a performance evaluation system from which the ground truth can be efficiently and accurately obtained indoors. The proposed scheme has exhibited robust tracking performance with significant reduction in average tracking error (up to 73.7%) compared to the traditional DR tracking method, in a practical indoor experimental testbed.

The rest of the paper is organized as follows. Section II summarizes the related works in the literature of DR-based pedestrian tracking. Section III describes the principle and implementation of state-of-the-art step-based DR scheme with an emphasis on arbitrary device orientation. Section IV discusses the proposed MAP algorithm for DR tracking error correction, together with its simplification, in detail. Section V presents the prototype implementation, experimental setup, results, and discussions. Finally, we conclude our work and point out future directions in Section VI.

II. Related Work

Both the fingerprinting-based approach and the trilateration-based approach for localization have been briefly introduced, with their challenges and limitations, in Section I. In this section, we focus on the relevant works in the literature of DR-based pedestrian tracking.

It has been shown experimentally in [9] that, double integration of accelerometer measurements introduces fast error accumulation over time. In order to overcome this cumulative error, ZUPT-based algorithms have been widely used in foot-mounted DR systems. For example, both [8] and [10] propose to reset the velocity error during the zero-velocity phase of each detected step, while [11] applies ZUPT as pseudo-measurements (observations), fed to an extended Kalman filter (EKF) for tracking error correction.

For the case of non-foot-mounted pedestrian DR systems, the step-based DR tracking approach is a preferable choice because it avoids double-integration. In the literature, most of the works which adopt this approach mount DR sensors on fixed parts of the user body with orientation which is convenient for DR. For example, [12] mounts the sensor module on the back of the pedestrian's waist. [13] mounts the sensor module on a helmet. However, there are also several works which implement DR tracking with arbitrary sensor placement and orientation in practical scenarios. For example, [14] proposes a simple algorithm to find the horizontal plane when the 3-axis accelerometer is oriented arbitrarily. In [15], the principal component analysis (PCA) technique is applied to find heading orientation, whose effectiveness is also verified experimentally by [16].

Note that, some works in the literature propose to facilitate DR initialization and DR error correction based on partial [17] or complete [18] location information provided by external infrastructure such as ultrasound or Wi-Fi systems. Although this paper focuses on a robust tracking scheme which involves only on-body sensors, external information can also be easily fused with our system to further improve the tracking performance.

III. Step-based Pedestrian Dead-Reckoning

The basic idea of the step-based DR tracking is to add the estimated current step displacement vector to the previously estimated location. In other words,

$$\mathbf{l}_k = \mathbf{l}_{k-1} + \mathbf{s}_k, \tag{1}$$

where $\mathbf{l}_{k-1}$ and $\mathbf{l}_k$ are the location estimates before and after the kth step, respectively. $\mathbf{s}_k$ is the estimated displacement vector for the kth step which is computed as,

$$\mathbf{s}_k = [\rho_k \cos\theta_k, \rho_k \sin\theta_k]^T, \tag{2}$$

where ρ_k and θ_k are the stride length and heading orientation for the kth step, respectively.

Despite the simple principle, implementing a practical step-based pedestrian DR system involves several important operations, namely, orientation projection, noise filtering, step detection, stride estimation, and heading determination. Next, we will describe how to realize these operations.

We have chosen two commercial smartphones, namely, the Google NexusOne and HTC Magic, for experimental data collection. Both phones have 3-axis accelerometer and 3-axis digital compass, whose data can be retrieved through the Android application programming interface (API).

Note that, our proposed method does not require the user to always carry two smartphones in practice. Instead, mobile devices such as a mobile phone, a tablet PC, or even a sensor

set embedded in a customized key chain, can be grouped flexibly to form multiple sensor sets.

A. Orientation Projection for Arbitrary Device Posture

Practically, the pedestrian may not fix the mobile device in such a way that the sensor axis is aligned to a convenient orientation for DR. Instead, devices such as mobile phones or PDAs are most likely to be placed with arbitrary orientation. Before further processing, the phone's acceleration measurements in its x-y-z local coordinate system need to be projected into the East-North-Up (E-N-U) world coordinate system using the digital compass' orientation measurements.

The three orientation measurements (pitch, roll, azimuth) reported by the Android API represent a sequence of rotations of the phone, starting from the initial orientation in which its x-y-z local coordinate system is aligned with the E-N-U world coordinate system. The three rotations are done in an extrinsic manner. Rotations about the Up axis (azimuth), the North axis (roll), and the East axis (pitch) are applied in sequence. In order to obtain the acceleration values in the world coordinate system, we multiply the inverse of the corresponding rotation matrices in the reversed order (inverse pitch, inverse roll, and inverse azimuth) to the acceleration vector reported in the local coordinate system.

B. Noise Filtering

Both the accelerometer and the digital compass in the smartphones give noisy measurements. In this paper, we adopt low-pass filters (LPF) for noise reduction. However, the fluctuating orientation measurements often experience sudden changes between two edge values such as 0 and 360 degrees, or -180 and 180 degrees. Applying LPF in these cases would cause the filtered measurements to be opposite or perpendicular to the true orientations. Therefore, we perform the filtering as follows. The raw acceleration measurements are passed into a pre-LPF with 200 ms window width. Next, the pre-filtered acceleration measurements are projected into the E-N-U world coordinate system, using the latest raw orientation measurements. Effects of the orientation noise are reduced by passing the projected accelerations to a post-LPF with 200 ms window width.

C. Step Detection

We utilize the acceleration measurements which have been projected into the vertical direction to detect steps, similar to [16]. Figure 1 shows the variations in projected and filtered vertical acceleration, for 12 steps taken at normal walking speed. The original data is collected by the HTC Magic phone, which is placed in one of the trousers side pocket. Note that larger variations are observed for every other local minimum, because the steps taken by the leg that is farther away from the pocket have smaller impact on the sensors.

The small peaks observed in the acceleration measurements are caused by residual sensor noise, random movements of sensor in pocket, and irregular human movements.

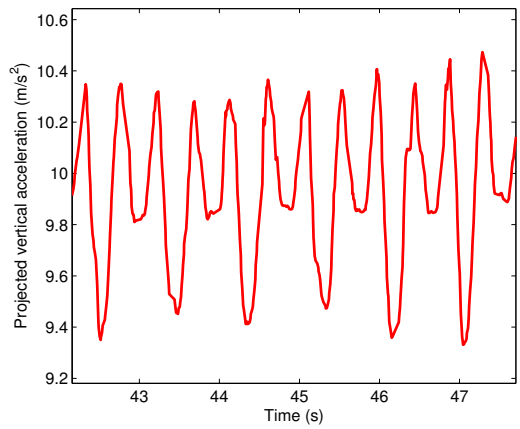

Figure 1. The acceleration variations in the vertical direction after projection.

In order to eliminate the effects of these peaks, we employ a relative threshold detection scheme. A new step is detected when a valid local maximum and a valid local minimum are detected in sequence. A local maximum is valid if it occurs at least 150 ms after the most recent valid local minimum, and the value of the local maximum exceeds that of the most recent local minimum by at least a threshold value, $\Delta_{\text{threshold}}$. Similarly, a local minimum is valid if it occurs at least 150 ms after the most recent valid local maximum, and the value of the local minimum is lower than that of the most recent local maximum by at least $\Delta_{\text{threshold}}$.

The choice of the 150 ms time difference threshold is due to the fact that, at normal walking speed, humans approximately take two steps per second, which leads to four or five peaks correspondingly. Therefore, it would be reasonable to pick 150 ms as the minimum inter-peak time difference. On the other hand, the detection threshold, $\Delta_{\text{threshold}}$, can be determined through calibrations.

D. Stride Length Estimation

Practically, stride length varies from step to step even for the same pedestrian. We use the model which was proposed in [19] and verified in [20] to estimate the stride length, ρ_k, from acceleration measurements for the kth step as,

$$\rho_k = K \cdot \sqrt[4]{a_k^{\text{v-max}} - a_k^{\text{v-min}}}, \tag{3}$$

where $a_k^{\text{v-max}}$ and $a_k^{\text{v-min}}$ are the maximum and minimum values of the projected vertical acceleration during the kth step, respectively. The constant K is dependent on each pedestrian, which can be determined through calibrations.

E. Heading Orientation

In [15], PCA is applied to the horizontal E-N plane to find the heading orientation, after the original accelerations are projected into the E-N-U world coordinate system. The same approach is verified in [16] experimentally. However, [16] uses a dedicated inertial measurement unit (IMU), with a data refreshing rate of 50 Hz. On the other hand, the low

cost sensors in our smartphones have a data updating rate of less than 25 Hz on average. Therefore, we only have fewer than half of the data samples compared to [16] for PCA-based heading detection, which delivers poor performance.

Limited by the low cost device's hardware data rate, we choose a different heading detection scheme. The adopted scheme performs trapezoidal-rule-based numerical integration over the acceleration readings that are projected into the E-N 2D plane, over the latest 1.4 seconds (for about two steps), in order to approximate the current heading direction.

IV. Proposed Method

After describing the principles and implementation of a practical step-based DR tracking system on a single mobile device, we proceed to discuss the proposed robust tracking algorithm in this section. We first formulate the robust tracking task as a MAP sensor fusion problem, whose solution can be sought for by constrained optimization. Taking into consideration the condition at which fusion is necessary, we prove that the constrained optimization problem can be converted to an unconstrained one. Finally, by making assumptions about the individual DR system's estimated variance, we refine the proposed scheme to a simple computation procedure.

A. System Architecture and Assumptions

Assume that the pedestrian is carrying two sets of sensors, labelled by set a and set b. Each set of sensors is able to perform DR location tracking on its own, with *independent tracking error*. Note that, the proposed robust tracking algorithm can easily be generalized to the case of more than two sets of sensors, under the independence assumption.

Assume that, the two sets of sensors are placed on the pedestrian's body with arbitrary but fixed orientations. More importantly, assume that the two sets of sensors have reasonably stable relative displacement with respect to each other. Mathematically speaking, if we let $\mathbf{l}_k^a$ and $\mathbf{l}_k^b$ denote the coordinates of locations for the two sets of sensors at the kth step, we have,

$$\mathbf{l}_k^a = \mathbf{m}_k^a + \mathbf{u}_k^a, \text{ and } \mathbf{l}_k^b = \mathbf{m}_k^b + \mathbf{u}_k^b, \tag{4}$$

where both $\mathbf{m}_k^a$ and $\mathbf{m}_k^b$ have deterministic and fixed displacements with respect to the center of pedestrian motion, while $\mathbf{u}_k^a$ and $\mathbf{u}_k^b$ are random vectors which account for the limited local random movements of the sensors. $\mathbf{u}_k^a$ and $\mathbf{u}_k^b$ are uniformly distributed within a spherical region centered at $\mathbf{0}$ with radii R_a and R_b, respectively. In order to simplify notations, assume $R_a = R_b = R$.

Based on this model, we can normalize $\mathbf{m}_k^a = \mathbf{m}_k^b = \mathbf{m}_k$, where $\mathbf{m}_k$ is the center of motion. Therefore the prior probability density function (pdf) for $\mathbf{l}_k^a$ and $\mathbf{l}_k^b$ is,

$$f(\mathbf{l}_k^a, \mathbf{l}_k^b) = \begin{cases} \alpha & \text{if } \|\mathbf{l}_k^a - \mathbf{l}_k^b\| \leq 2R, \\ 0 & \text{otherwise,} \end{cases} \tag{5}$$

where α is a constant whose value is dependent on the dimension of the tracking problem and the radius of uncertainty region, R.

B. The Robust Tracking Algorithm

1) Initialization: The DR system alone is only able to estimate the displacement vector but not the initial location. In order to initialize the DR pedestrian tracking, knowledge of the initial location, $\mathbf{m}_0$, must be provided to the DR system through either user indication or some other localization system. Discussions on utilizing extra information and other technology for initial location knowledge is beyond the scope of this paper. Interested readers may refer to [17] and [18] for more information.

Recall that, $\mathbf{m}_k^a = \mathbf{m}_k + \mathbf{u}_k^a$ and $\mathbf{m}_k^b = \mathbf{m}_k + \mathbf{u}_k^b$ are the locations of the two sets of sensors after the fixed displacements with respect to the center of motion are normalized. In order to initialize, we conveniently assume that, $\mathbf{u}_0^a = \mathbf{u}_0^b = \mathbf{0}$. Therefore, $\mathbf{l}_0^a = \mathbf{l}_0^b = \mathbf{m}_0$.

2) Maximum A Posteriori Sensor Fusion: Let $\hat{\mathbf{l}}_k^a$ and $\hat{\mathbf{l}}_k^b$ denote the DR estimates reported by the two sets of sensors independently at the kth step. The DR task is to find $\mathbf{l}_k^a$ and $\mathbf{l}_k^b$ which maximize the a posteriori pdf, $f(\mathbf{l}_k^a,\ \mathbf{l}_k^b \mid \hat{\mathbf{l}}_k^a,\ \hat{\mathbf{l}}_k^b)$.

From this point onwards, we can drop the index term k for simplicity of representation without causing any confusion, because the following discussions are all about the kth step.

According to the Bayes' Theorem, we have,

$$f(\mathbf{l}^a,\ \mathbf{l}^b \mid \hat{\mathbf{l}}^a,\ \hat{\mathbf{l}}^b) = \frac{f(\hat{\mathbf{l}}^a,\ \hat{\mathbf{l}}^b \mid \mathbf{l}^a,\ \mathbf{l}^b) \cdot f(\mathbf{l}^a,\ \mathbf{l}^b)}{f(\hat{\mathbf{l}}^a,\ \hat{\mathbf{l}}^b)}. \tag{6}$$

Because the two sets of sensors provide independent DR estimates, we have,

$$f(\mathbf{l}^a,\ \mathbf{l}^b \mid \hat{\mathbf{l}}^a,\ \hat{\mathbf{l}}^b) = \frac{f(\hat{\mathbf{l}}^a \mid \mathbf{l}^a) \cdot f(\hat{\mathbf{l}}^b \mid \mathbf{l}^b) \cdot f(\mathbf{l}^a,\ \mathbf{l}^b)}{f(\hat{\mathbf{l}}^a,\ \hat{\mathbf{l}}^b)}. \tag{7}$$

On the right hand side of (7), the evidence pdf in the denominator, $f(\hat{\mathbf{l}}^a,\ \hat{\mathbf{l}}^b)$, is not affected by the choice of either $\mathbf{l}^a$ or $\mathbf{l}^b$. Therefore, maximizing $f(\mathbf{l}^a,\ \mathbf{l}^b \mid \hat{\mathbf{l}}^a,\ \hat{\mathbf{l}}^b)$ is equivalent to maximizing $f(\hat{\mathbf{l}}^a \mid \mathbf{l}^a) \cdot f(\hat{\mathbf{l}}^b \mid \mathbf{l}^b) \cdot f(\mathbf{l}^a,\ \mathbf{l}^b)$.

The terms $f(\hat{\mathbf{l}}^a \mid \mathbf{l}^a)$ and $f(\hat{\mathbf{l}}^b \mid \mathbf{l}^b)$ are the likelihood pdfs, which are the pdfs of observing $\hat{\mathbf{l}}^a$ and $\hat{\mathbf{l}}^b$, conditioned on the actual locations, $\mathbf{l}^a$ and $\mathbf{l}^b$, respectively. Due to the residual noise in filtered sensor measurements and irregularity in pedestrian body movements, each step's displacement is estimated with independent error. The likelihood pdf for the DR estimation over a few steps can therefore be modelled as Gaussian, according to the Central Limit Theorem (CLT).

Therefore, both $f(\hat{\mathbf{l}}^a \mid \mathbf{l}^a)$ and $f(\hat{\mathbf{l}}^b \mid \mathbf{l}^b)$ are Gaussian. The prior pdf $f(\mathbf{l}^a,\ \mathbf{l}^b)$ in (5) is a positive constant within a spherical region and 0 elsewhere. The robust tracking task thus becomes a constrained optimization problem as,

$$\begin{aligned} \underset{\mathbf{l}^a, \mathbf{l}^b}{\text{maximize}} \quad & f(\hat{\mathbf{l}}^a \mid \mathbf{l}^a) \cdot f(\hat{\mathbf{l}}^b \mid \mathbf{l}^b) \\ \text{subject to} \quad & \|\mathbf{l}^a - \mathbf{l}^b\| \leq 2R. \end{aligned}$$

We further observe that there can only be two cases in which the maximal value is obtained.

In the first case, $\|\hat{\mathbf{l}}^a - \hat{\mathbf{l}}^b\| \leq 2R$. As a result, both Gaussian pdfs can obtain their maximal values (hence their product is maximized) at $\tilde{\mathbf{l}}^a = \hat{\mathbf{l}}^a$ and $\tilde{\mathbf{l}}^b = \hat{\mathbf{l}}^b$, while satisfying $f(\tilde{\mathbf{l}}^a,\ \tilde{\mathbf{l}}^b) \neq 0$. However, in this case, because the optimal $\tilde{\mathbf{l}}^a$ and $\tilde{\mathbf{l}}^b$ are close to each other, it is not necessary for the fusion to take place.

In the second case, $\|\hat{\mathbf{l}}^a - \hat{\mathbf{l}}^b\| > 2R$. The estimates of the two sets of sensors deviate from each to such an extent that error correction needs to be done. In order to satisfy that $f(\mathbf{l}^a,\ \mathbf{l}^b) \neq 0$, the distance between the optimal $\tilde{\mathbf{l}}^a$ and $\tilde{\mathbf{l}}^b$ must be $2R$ in this case. This can be proven, almost trivially, by contradiction as follows. For simplicity, we only consider the 2-D case here.

Proof: Given that, $\|\hat{\mathbf{l}}^a - \hat{\mathbf{l}}^b\| > 2R$, and $f(\hat{\mathbf{l}}^a|\ \mathbf{l}^a) \cdot f(\hat{\mathbf{l}}^b|\ \mathbf{l}^b)$ is maximized at $\mathbf{l}^a = \tilde{\mathbf{l}}^a$ and $\mathbf{l}^b = \tilde{\mathbf{l}}^b$, respectively, which satisfy $\|\tilde{\mathbf{l}}^a - \tilde{\mathbf{l}}^b\| = d < 2R$. Draw two circles C_a and C_b centered at $\tilde{\mathbf{l}}^a$ and $\tilde{\mathbf{l}}^b$ with arbitrarily small radii ϵ_a and ϵ_b, respectively, such that $\epsilon_a + \epsilon_b + d < 2R$. If any point on C_a or C_b results in a larger $f(\hat{\mathbf{l}}^a|\ \mathbf{l}^a) \cdot f(\hat{\mathbf{l}}^b|\ \mathbf{l}^b)$, it would contradict with the condition that $\tilde{\mathbf{l}}^a$ and $\tilde{\mathbf{l}}^a$ are the optimal feasible points. Therefore, both $\tilde{\mathbf{l}}^a$ and $\tilde{\mathbf{l}}^b$ must be the local maximum of the likelihood pdfs $f(\hat{\mathbf{l}}^a|\ \mathbf{l}^a)$ and $f(\hat{\mathbf{l}}^b|\ \mathbf{l}^b)$, respectively. However, each Gaussian pdf has only one local maximum which is also the global maximum in nature. Therefore, $\tilde{\mathbf{l}}^a = \hat{\mathbf{l}}^a$ and $\tilde{\mathbf{l}}^b = \hat{\mathbf{l}}^b$, which contradicts with the fact that $\|\hat{\mathbf{l}}^a - \hat{\mathbf{l}}^b\| > 2R$. Therefore, we must have, $\|\tilde{\mathbf{l}}^a - \tilde{\mathbf{l}}^b\| = 2R$. ■

Therefore, the constrained optimization problem becomes,

$$\begin{aligned} \underset{\mathbf{l}^a,\mathbf{l}^b}{\text{maximize}} \quad & f(\hat{\mathbf{l}}^a|\ \mathbf{l}^a) \cdot f(\ \hat{\mathbf{l}}^b|\ \mathbf{l}^b) \\ \text{subject to} \quad & \|\mathbf{l}^a - \mathbf{l}^b\| = 2R. \end{aligned}$$

In order to solve it, let,

$$\begin{aligned} \mathbf{l}^b &= \mathbf{l}^a + \mathbf{q} \\ &= [x_a + 2R\cos\phi,\ y_a + 2R\sin\phi]^T, \end{aligned} \tag{8}$$

which eliminates the constraint and adds one more free variable, ϕ, to the maximization problem.

The objective function to be maximized can thus be written as,

$$\begin{aligned} F &= f(\hat{\mathbf{l}}^a|\ \mathbf{l}^a) \cdot f(\ \hat{\mathbf{l}}^b|\ \mathbf{l}^b) \\ &= f(\hat{\mathbf{l}}^a|\ \mathbf{l}^a) \cdot f(\ \hat{\mathbf{l}}^b|\ \mathbf{l}^a + \mathbf{q}) \\ &= Q \cdot \exp[G], \end{aligned} \tag{9}$$

where,

$$Q = \frac{1}{4\pi^2 \cdot |\mathbf{\Sigma}_a|^{\frac{1}{2}} \cdot |\mathbf{\Sigma}_b|^{\frac{1}{2}}}, \tag{10}$$

and $\mathbf{\Sigma}_a$ and $\mathbf{\Sigma}_b$ are the covariance matrices for the Gaussian pdfs $f(\hat{\mathbf{l}}^a|\ \mathbf{l}^a)$ and $f(\hat{\mathbf{l}}^b|\ \mathbf{l}^b)$, respectively. We also have,

$$\begin{aligned} G = &-\frac{1}{2}(\mathbf{l}^a - \hat{\mathbf{l}}^a)^T \mathbf{\Sigma}_a^{-1}(\mathbf{l}^a - \hat{\mathbf{l}}^a) - \\ &\frac{1}{2}(\mathbf{l}^a + \mathbf{q} - \hat{\mathbf{l}}^b)^T \mathbf{\Sigma}_b^{-1}(\mathbf{l}^a + \mathbf{q} - \hat{\mathbf{l}}^b). \end{aligned} \tag{11}$$

At the optimal point, we have the equalities,

$$\frac{\partial F}{\partial x_a} = 0,\ \frac{\partial F}{\partial y_a} = 0,\ \frac{\partial F}{\partial \phi} = 0. \tag{12}$$

Correspondingly, we have,

$$\frac{\partial F}{\partial G} \cdot [\frac{\partial G}{\partial \mathbf{l}^a}]^T \cdot \frac{\partial \mathbf{l}^a}{\partial x_a} = 0, \tag{13}$$

$$\frac{\partial F}{\partial G} \cdot [\frac{\partial G}{\partial \mathbf{l}^a}]^T \cdot \frac{\partial \mathbf{l}^a}{\partial y_a} = 0, \tag{14}$$

$$\frac{\partial F}{\partial G} \cdot [\frac{\partial G}{\partial \mathbf{q}}]^T \cdot \frac{\partial \mathbf{q}}{\partial \phi} = 0. \tag{15}$$

The term, $\frac{\partial F}{\partial G} = Q \cdot \exp[G]$, is always nonzero. Therefore, we can ignore it in further discussions.

The term $\frac{\partial G}{\partial \mathbf{l}^a}$ is evaluated as,

$$\frac{\partial G}{\partial \mathbf{l}^a} = -\mathbf{\Sigma}_a^{-1}(\mathbf{l}^a - \hat{\mathbf{l}}^a) - \mathbf{\Sigma}_b^{-1}(\mathbf{l}^a + \mathbf{q} - \hat{\mathbf{l}}^b). \tag{16}$$

Let,

$$\mathbf{l}^a = [x_a, y_a]^T,\ \hat{\mathbf{l}}_a = [\hat{x}_a, \hat{y}_a]^T,\ \hat{\mathbf{l}}_b = [\hat{x}_b, \hat{y}_b]^T. \tag{17}$$

We have,

$$\frac{\partial \mathbf{l}^a}{\partial x_a} = [1, 0]^T,\ \text{and}\ \frac{\partial \mathbf{l}^a}{\partial y_a} = [0, 1]^T. \tag{18}$$

The term $\frac{\partial G}{\partial \mathbf{q}}$ is evaluated as,

$$\frac{\partial G}{\partial \mathbf{q}} = -\mathbf{\Sigma}_b^{-1}(\mathbf{l}^a + \mathbf{q} - \hat{\mathbf{l}}^b). \tag{19}$$

The term $\frac{\partial \mathbf{q}}{\partial \phi}$ is evaluated as,

$$\frac{\partial \mathbf{q}}{\partial \phi} = [-2R\sin\phi,\ 2R\cos\phi]^T. \tag{20}$$

For specific $\hat{\mathbf{l}}^a$, $\hat{\mathbf{l}}^b$, $\mathbf{\Sigma}_a$, and $\mathbf{\Sigma}_b$, (13) to (15) give us three linear equations, which can be solved for x_a, y_a, and ϕ.

However, the covariance matrices, $\mathbf{\Sigma}_a$ and $\mathbf{\Sigma}_b$, for DR estimates, are difficult to evaluate. Therefore, we further assume that,

$$\mathbf{\Sigma}_a = \sigma^2\mathbf{I},\ \text{and}\ \mathbf{\Sigma}_b = \sigma^2\mathbf{I}. \tag{21}$$

Following this assumption, we can simplify (13) to (15) as,

$$x_a - \hat{x}_a + x_a - \hat{x}_b + 2R\cos\phi = 0, \tag{22}$$

$$y_a - \hat{y}_a + y_a - \hat{y}_b + 2R\sin\phi = 0, \tag{23}$$

$$x_a\sin\phi - \hat{x}_b\sin\phi - y_a\cos\phi + \hat{y}_b\cos\phi = 0. \tag{24}$$

Combining (22) and (23) gives us,

$$\tan\phi = \frac{y_a - \hat{y}_b + y_a - \hat{y}_a}{x_a - \hat{x}_b + x_a - \hat{x}_a}. \tag{25}$$

Divide (24) by $\cos\phi$ gives us,

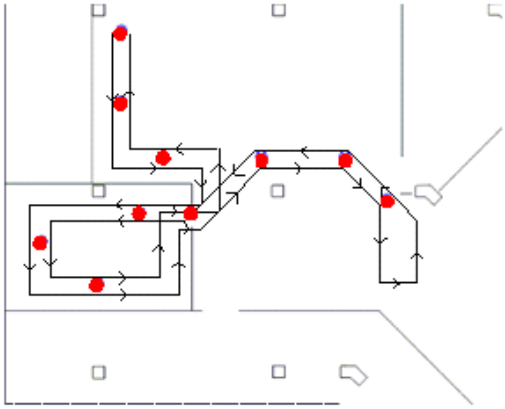

Figure 2. Map of the indoor testbed. The arrowed lines sketch the walking path, and the shaded circles indicate the locations of the waypoints.

$$\tan\phi = \frac{y_a - \hat{y}_b}{x_a - \hat{x}_b}. \tag{26}$$

Combining (25) and (26) we have,

$$\tan\phi = \frac{y_a - \hat{y}_b}{x_a - \hat{x}_b} = \frac{y_a - \hat{y}_a}{x_a - \hat{x}_a}. \tag{27}$$

The result in (27) implies that $\mathbf{l}^a = [x_a, y_a]^T$ lies on the line that connects $\hat{\mathbf{l}}^a$ and $\hat{\mathbf{l}}^b$.

Moreover, rewriting (22) and (23), we have,

$$x_a = \frac{\hat{x}_a + \hat{x}_b}{2} - R\cos\phi,\ \ y_a = \frac{\hat{y}_a + \hat{y}_b}{2} - R\sin\phi, \tag{28}$$

which means the optimal $\mathbf{l}^a$ is on the line segment that connects $\hat{\mathbf{l}}^a$ and $\hat{\mathbf{l}}^b$ with distance R away from the middle point of that line segment.

Consequently, the optimal $\mathbf{l}^b$ is also on the line segment that connects $\hat{\mathbf{l}}^a$ and $\hat{\mathbf{l}}^b$ with distance R away from the middle point of that line segment, on the other side of $\mathbf{l}^a$.

V. Experimental Results and Discussions

A. Testbed Setup and Experimental Devices

In order to evaluate the performance of the proposed scheme, we setup an indoor testbed which spans an area of 140 m^2 in one laboratory on campus, as shown in Fig. 2. Numerous desktop computers and metal cabinets are scattered in the testbed. They distort the Earth's magnetic fields, which disturb the digital compass readings.

As shown in the same figure, an indoor walking path is picked in our testbed. The path covers about 90 m in total distance, with various obstacles and turns. It takes about 2 minutes to walk along it, under normal indoor walking speed. Note that, actual distances covered and time taken for travel vary across different experimental trials.

Three smartphones with Android operating system are carried by a pedestrian for data collection and experiment control purpose, as shown in Fig. 3. All the phones are equipped with Wi-Fi modules which connect to the same wireless LAN for communication purpose.

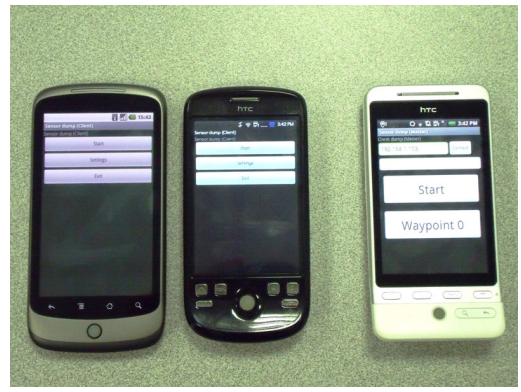

Figure 3. Experimental data collection devices. From left to right: Google NexusOne (Worker 1); HTC Magic (Worker 2); HTC Hero (Manager).

Two of the three phones, which are referred to as the "worker" devices, are placed in the pedestrian's two trousers pockets. They are both equipped with 3-axis accelerometers and 3-axis magnetometers. We program them to record their sensor readings and timestamps at the highest possible rate ($<$ 25 Hz), and transmit them back through wireless connections. Note that, in this case, the radius R for both phones' local random movements about the center of motion, is set to 0.075 m. The third phone is referred to as the "manager" device, which is hand-held by the pedestrian. We install programs for the pedestrian to control the experiment and record ground truth in the "manager".

B. System Synchronization

All the three smartphones record data using their own local clock with millisecond time resolution. The synchronization between the phones is performed as follows. As soon as the pedestrian tabs the "Start" button on the "manager", it records down its local timestamp T_1, and sends out a START message to both the "workers". The ith "worker" records its local timestamp, T_2^i, and replies with an ACK message immediately, when it receives the START message. The manager records down the local timestamp T_3^i when the ACK message is received from the ith "worker". We assume both the START message and ACK message between "manager" and the same "worker" takes the same amount of transmission time. Therefore, to synchronize with the ith "worker", the manager subtracts $(T_1 + T_3^i)/2$ from all of its local timestamps. On the other hand, the ith "worker" subtracts T_2^i from all of its local timestamps in order to synchronize with the "manager".

C. Ground Truth Collection

There are mainly two methods to collect ground truth for performance evaluation in the DR-based pedestrian tracking literature. The first method uses location coordinates provided by GPS [13]. It works only in the outdoor scenario. Moreover, commercial GPS's location estimation itself is subject to considerable error. The second method obtains

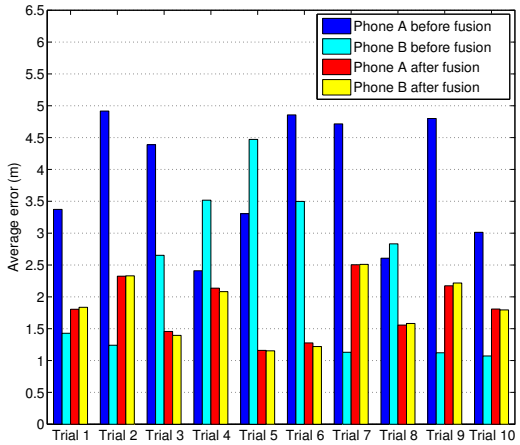

Figure 4. Average tracking errors before and after fusion for 10 experimental trials.

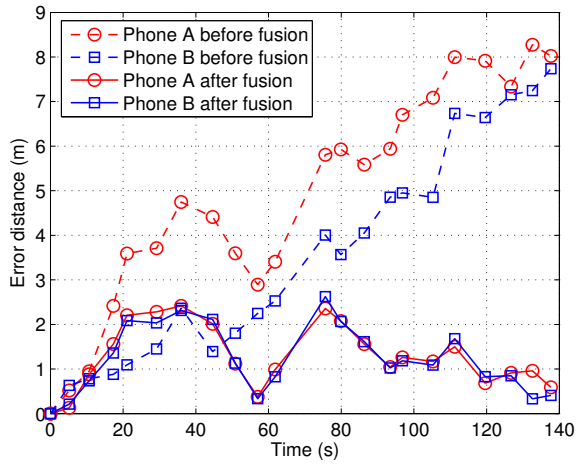

Figure 5. Temporal error propagation before and after fusion for Trial 6.

ground truth relying on a reference DR unit [16], which is built on top of dedicated hardware with low noise and good updating rate. It can be foot-mounted on the tester so that ZUPT can be applied for noise cancellation. However, this approach is expensive and the reference DR system is still subject to error propagation over time.

For our experiment, we developed an efficient approach to collect accurate ground truth indoors, utilizing the "manager" phone and testbed setup. Along the walking path we have marked 10 distinctive locations as waypoints on the floor. Because each waypoint location is reached twice or thrice following the walking path, ground truth can be recorded and referred to for a total of 22 times in one walking trial. Note that, in order to maintain natural walking behavior, the pedestrians who participate in the experiment are not required to follow the path strictly as sketched in the figure, nor do they have to step on the waypoint locations precisely, as long as all the waypoints are *passed through exactly in the correct sequence*.

The pedestrian starts one trial of experiment by tabbing the "Start" button on the touch screen of the "manager". The "manager" will instantly order both the "workers" to start sensor data collection through wireless connection. Whenever the pedestrian is passing through a certain waypoint on the walking path, he will tab the "Waypoint" button on the touch screen of the "manager", which will record the timestamp of this particular instance of passing. Therefore, 22 pieces of ground truth with timestamps can be collected accurately and efficiently for each trial of experiment. The estimated location, at the instance when a certain actual waypoint is passed by, can be compared to the actual waypoint location for error distance computation.

D. Tracking Performance

Fig. 4 shows the average location tracking error delivered by the two "worker" phones, before and after the proposed fusion algorithm is applied, for 10 experimental trials. As shown in the figure, the effects of the proposed scheme can be categorized into two different scenarios.

In the first scenario (Trial 3, 4, 5, 6, and 8), both phones' average tracking errors using traditional DR have been significantly reduced with our proposed fusion scheme. The largest error reduction rate is reported in Trial 6 at 73.7%. We show the error propagation (Fig. 5) and actual tracking paths (Fig. 6) for this trial, as an example here. Fig. 6 shows that, individual DR systems of the two phones exhibit adverse error biases in location tracking estimates. On the other hand, Fig. 5 shows that the difference between the magnitudes of the two phones' (adverse) error biases is not so big. Therefore, the proposed scheme effectively cancels these error biases out, leaving small residual errors. As a result, the tracking errors of the proposed scheme for both phones are significantly smaller than those before fusion.

In the second scenario (Trial 1, 2, 7, 9, 10), the proposed algorithm delivers intermediate tracking performance, with average errors in between those of the two phones' individual DR systems. Here, we show the error propagation (Fig. 7) and actual tracking paths (Fig. 8) for Trial 7, as an example. Fig. 8 has shown that, the two phones still give adverse error biases in location tracking estimates, as in the previous scenario. On the other hand, Fig. 7 has shown that, the difference between the magnitudes of the two phones' (adverse) error biases is much larger than before; Phone B's DR tracking error before fusion happens to be very small in this particular trial. Therefore, even after the proposed scheme cancels part of the error bias out, a large residual error bias is still left in the fused results. Therefore, the tracking errors of the proposed scheme for the two phones are between those of the two phone's original DR systems.

However, we argue that, the proposed scheme is still useful in the second scenario, for two reasons. First, in practical application scenarios, it is hard, if not impossible, for the pedestrian user to tell which one of the multiple

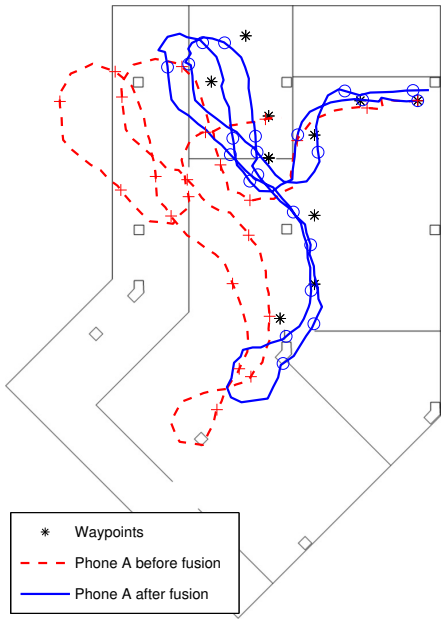

(a) Tracking paths before and after fusion for phone A.

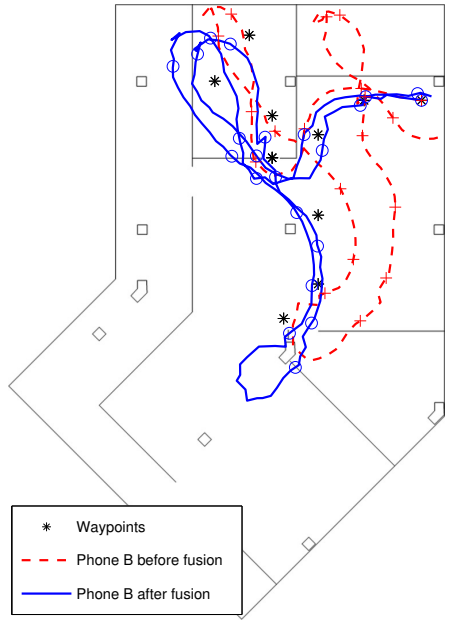

(b) Tracking paths before and after fusion for phone B.

Figure 6. Tracking paths before and after fusion for Trial 6.

devices is providing better tracking performance. Second, the absolute error reduced by the proposed scheme, from the more erroneous phone, is significantly larger than the error that it has raised, from the phone with small original errors. Overall, the proposed scheme is still giving robust and stable tracking performance.

VI. Conclusion and Future Work

In conclusion, we have proposed a robust pedestrian tracking system, exploiting the stability of inter-device relative displacements, in commercial mobile devices containing DR-capable sensors. We have derived the robust tracking algorithm in general and specialized it to a simple computation procedure. A prototype of the proposed system, as well as an efficient and accurate ground truth collection system have been implemented with accompanying performance evaluation. The proposed scheme has shown significant performance improvement in a realistic indoor testbed.

We point out two future directions. First, we have assumed equal variance for different DR systems in this paper and performed experiments with devices placed symmetrically in the pedestrian's body. A real-time scheme which approximates the estimates' variance would make the proposed scheme more accessible. Moreover, map-matching schemes, and/or external localization technologies can also be fused into the proposed scheme to further reduce tracking error and provide initial location information.

Acknowledgment

This work is supported by National Research Foundation project grant NRF2007IDM-IDM002-069 on "Life Spaces".

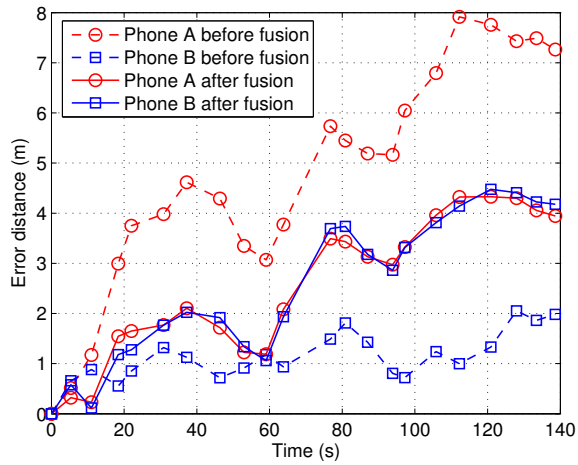

Figure 7. Temporal error propagation before and after fusion for Trial 7.

References

[1] H. Zang, F. Baccelli, and J. Bolot, "Bayesian inference for localization in cellular networks," in *Proc. IEEE INFOCOM*, Mar. 2010, pp. 1963–1971.

[2] P. Bahl and V. Padmanabhan, "RADAR: An in-building RF-based user location and tracking system," in *Proc. IEEE INFOCOM*, Mar. 2000, pp. 775–784.

[3] A. Kushki, K. N. Plataniotis, and A. N. Venetsanopoulos, "Kernel-based positioning in wireless local area networks," *IEEE Trans. Mobile Computing*, vol. 6, no. 6, pp. 689–705, Jun. 2007.

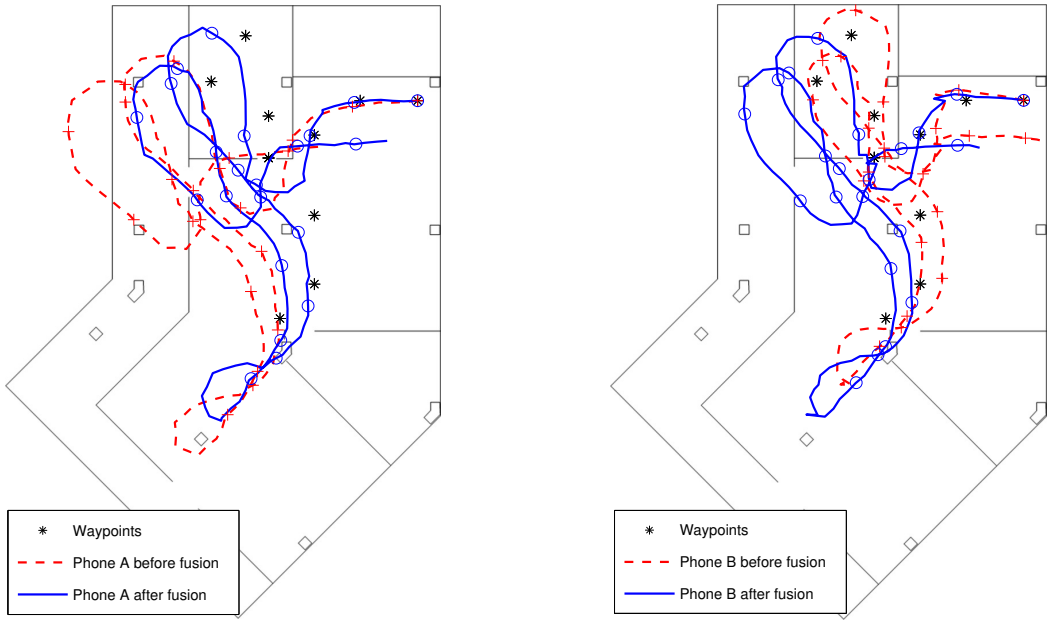

(a) Tracking paths before and after fusion for phone A.

(b) Tracking paths before and after fusion for phone B.

Figure 8. Tracking paths before and after fusion for Trial 7.

[4] N. B. Priyantha, A. Chakraborty, and H. Balakrishnan, "The Cricket location-support system," in *Proc. ACM MOBICOM*, Aug. 2000, pp. 32–43.

[5] R. Yamasaki, A. Ogino, T. Tamaki, T. Uta, N. Matsuzawa, and T. Kato, "TDOA location system for IEEE 802.11b WLAN," in *Proc. IEEE WCNC*, Mar. 2005, pp. 2338–2343.

[6] S. A. Golden and S. S. Bateman, "Sensor measurements for Wi-Fi location with emphasis on time-of-arrival ranging," *IEEE Trans. Mobile Computing*, vol. 6, no. 10, pp. 1185–1198, Oct. 2007.

[7] H. Lim, L.-C. Kung, J. C. Hou, and H. Luo, "Zero-configuration, robust indoor localization: theory and experimentation," in *Proc. IEEE INFOCOM*, Apr. 2006, pp. 405–420.

[8] E. Foxlin, "Pedestrian tracking with shoe-mounted inertial sensors," *IEEE Computer graphics and applications*, vol. 25, no. 6, pp. 38–46, Nov.-Dec. 2005.

[9] Y. K. Thong, M. S. Woolfson, J. A. Crowe, B. R. Hayes-Gill, and R. E. Challis, "Dependence of inertial measurements of distance on accelerometer noise," pp. 1163–1172, 2002.

[10] S. Beauregard, "Omnidirectional pedestrian navigation for first responders," in *Proc. IEEE WCNC*, Mar. 2007, pp. 33–36.

[11] L. Ojeda and J. Borenstein, "Personal dead-reckoning system for GPS-denied environents," in *Proc. IEEE SSRR*, Sep. 2007, pp. 1–6.

[12] L. Fang, P. J. Antsaklis, L. A. Montestruque, M. B. McMickell, M. Lemmon, Y. Sun, H. Fang, I. Koutroulis, M. Haenggi, M. Xie, and X. Xie, "Design of a wireless assisted pedestrian dead reckoning system –The NavMote experience," *IEEE Trans. Instrumentation and Measurement*, vol. 54, no. 6, pp. 2342–2358, Dec. 2005.

[13] S. Beauregard, "A helmet-mounted pedestrian dead reckoning system," in *Proc. IFAWC*, Mar. 2006.

[14] D. Mizell, "Using gravity to estimate accelerometer orientation," in *Proc. IEEE ISWC*, Nov. 2003, pp. 252–253.

[15] K. Kunze, P. Lukowicz, K. Partridge, and B. Begole, "Which way am I facing: inferring horizontal device orientation from an accelerometer signal," in *Proc. IEEE ISWC*, Sep. 2009, pp. 149–150.

[16] U. Steinhoff and B. Schiele, "Dead reckoning from the pocket - an experimental study," in *Proc. IEEE PERCOM*, Mar. 2010, pp. 162–170.

[17] Y. Jin, M. Motani, W.-S. Soh, and J. Zhang, "SparseTrack: Enhancing indoor pedestrian tracking with sparse infrastructure support," in *Proc. IEEE INFOCOM*, Mar. 2010, pp. 1–9.

[18] H. Wang, H. Lenz, A. Szabo, J. Bamberger, and U. D. Hanebeck, "WLAN-Based pedestrian tracking using particle filters and low-cost MEMS sensors," in *Proc. IEEE WPNC*, Mar. 2007, pp. 1–9.

[19] H. Weinberg, "Using the ADX1202 in pedometer and personal navigation applications," 2002.

[20] D. Alvarez, R. C. Gonzaléz, A. López, and J. C. Alvarez, "Comparison of step length estimators from wearable accelerometer devices," in *Proc. IEEE EMBS*, Aug. 2006, pp. 5964–5967.